Report

Cell Reports

Structure and Functional Binding Epitope of V-domain Ig Suppressor of T Cell Activation

Graphical Abstract

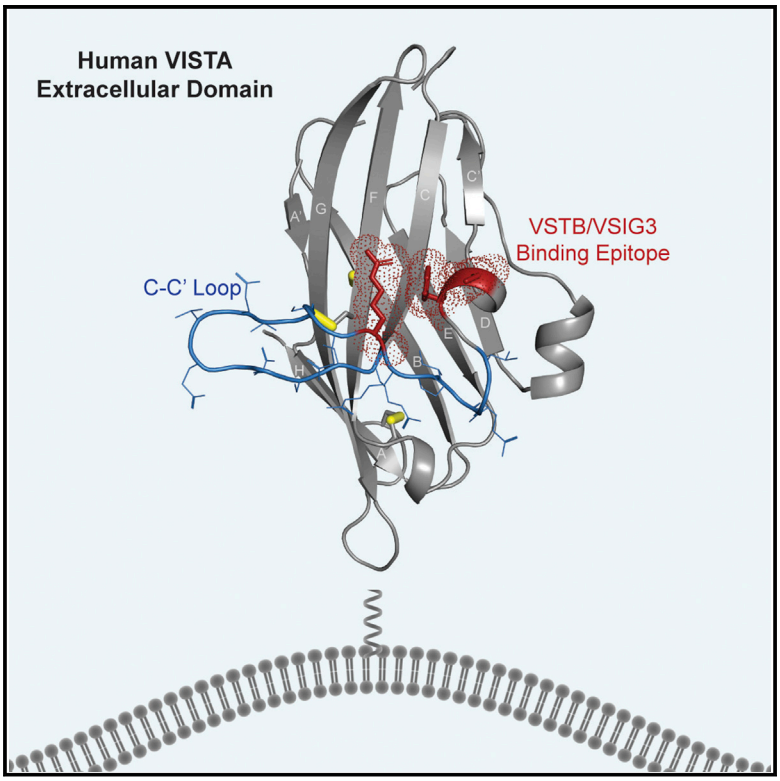

Highlights

- The crystal structure of the human VISTA extracellular domain was determined
- VISTA contains two unique disulfides and an extended C-C′ loop
- The epitope of an inhibitor antibody was mapped to a three-residue surface
- The antibody epitope was found to overlap with the VISTA-VSIG3 binding interface

Authors

Nishant Mehta, Sainiteesh Maddineni, Irimpan I. Mathews, R. Andres Parra Sperberg, Po-Ssu Huang, Jennifer R. Cochran

Correspondence

possu@stanford.edu (P.-S.H.), cochran1@stanford.edu (J.R.C.)

In Brief

Using a combinatorial MR-Rosetta approach, Mehta et al. solve the crystal structure of human V-domain immunoglobulin (Ig) suppressor of T cell activation (VISTA), an important checkpoint protein in cancer immunotherapy. The authors use yeast display to map the epitope of a clinical anti-VISTA antibody and demonstrate its overlap to the VISTA/V-set and Ig domain containing 3 (VSIG3) binding interface.

Mehta et al., 2019, Cell Reports *28*, 2509–2516
September 3, 2019
https://doi.org/10.1016/j.celrep.2019.07.073

CellPress

Cell Reports
Report

Structure and Functional Binding Epitope of V-domain Ig Suppressor of T Cell Activation

Nishant Mehta,[1] Sainiteesh Maddineni,[1] Irimpan I. Mathews,[2] R. Andres Parra Sperberg,[1] Po-Ssu Huang,[1,*] and Jennifer R. Cochran[1,3,4,*]

[1]Department of Bioengineering, Stanford University, Stanford, CA 94305, USA
[2]Stanford Synchrotron Radiation Laboratory, 2575 Sand Hill Road, Menlo Park, CA 94025, USA
[3]Department of Chemical Engineering, Stanford University, Stanford, CA 94305, USA
[4]Lead Contact
*Correspondence: possu@stanford.edu (P.-S.H.), cochran1@stanford.edu (J.R.C.)
https://doi.org/10.1016/j.celrep.2019.07.073

SUMMARY

V-domain immunoglobulin (Ig) suppressor of T cell activation (VISTA) is an immune checkpoint protein that inhibits the T cell response against cancer. Similar to PD-1 and CTLA-4, a blockade of VISTA promotes tumor clearance by the immune system. Here, we report a 1.85 Å crystal structure of the elusive human VISTA extracellular domain, whose lack of homology necessitated a combinatorial MR-Rosetta approach for structure determination. We highlight features that make the VISTA immunoglobulin variable (IgV)-like fold unique among B7 family members, including two additional disulfide bonds and an extended loop region with an attached helix that we show forms a contiguous binding epitope for a clinically relevant anti-VISTA antibody. We propose an overlap of this antibody-binding region with the binding epitope for V-set and Ig domain containing 3 (VSIG3), a purported functional binding partner of VISTA. The structure and functional epitope presented here will help guide future drug development efforts against this important checkpoint target.

INTRODUCTION

V-domain immunoglobulin (Ig) suppressor of T cell activation (VISTA) is an immune checkpoint protein involved in the regulation of T cell activity. VISTA is highly expressed on myeloid-derived cells such as CD11b+ monocytes, CD11c+ dendritic cells, and, to a lesser extent, CD4+ and CD8+ T cells (Wang et al., 2011). Similar to the well-studied PD-1, PD-L1, and CTLA-4 checkpoint proteins, the presence of VISTA results in reduced T cell activation and proliferation. The mechanism of action for this effect, however, is unclear, as VISTA has been thought to function as both a ligand and a receptor. As a ligand, VISTA is expressed on antigen-presenting cells and binds an unknown receptor on T cells to inhibit downstream T cell activation (Lines et al., 2014; Wang et al., 2011). As a receptor, VISTA is expressed on T cells and transduces intracellular inhibitory signals after ligand binding to curtail T cell activity (Flies et al., 2014, 2015). A proposed ligand for VISTA has recently been identified as V-set and Ig domain containing 3 (VSIG3) (Wang et al., 2019; Yang et al., 2017).

Checkpoint proteins have been found to be overexpressed by cancer cells or their surrounding immune cells and prevent anti-tumor activity by co-opting natural regulation mechanisms to escape immune clearance. In particular, VISTA is upregulated on tumor-infiltrating leukocytes, including high expression on myeloid-derived suppressor cells (MDSCs) (Le Mercier et al., 2014; Wang et al., 2018). Through VISTA signaling, these inhibitory immune cells prevent effective antigen presentation and indirectly promote tumor growth. VISTA is implicated in a number of human cancers, including skin (melanoma) (Kakavand et al., 2017), prostate (Gao et al., 2017), colon (Xie et al., 2018), pancreatic (Liu et al., 2018), ovarian (Mulati et al., 2019), endometrial (Mulati et al., 2019), and lung (NSCLC) (Villarroel-Espindola et al., 2018). Additionally, VISTA levels have been found to increase after anti-CTLA-4 treatment in prostate cancer (Gao et al., 2017) and after anti-PD-1 treatment in metastatic melanoma (Kakavand et al., 2017), highlighting VISTA expression as a method of acquired resistance to currently available checkpoint inhibitors. For these reasons, VISTA is an important cancer immunotherapy target for drug development efforts.

The human VISTA protein is 279 amino acids in length, comprising a 162-amino-acid extracellular domain, a 21-amino-acid transmembrane domain, and a 96-amino-acid cytoplasmic domain. The cytoplasmic domain lacks any immunoreceptor tyrosine-based signaling motifs but does contain multiple casein kinase 2 and phosphokinase C phosphorylation sites that could play a role in signal transduction. Protein sequence analysis has clustered VISTA with the B7 family group of ligands (CD80, CD86, PD-L1, PD-L2, ICOSL, and CD276), all of which contain a conserved immunoglobulin variable (IgV)-like fold. The closest homolog within the B7 family is PD-L1, which shares a modest 23% sequence identity with VISTA. The VISTA extracellular domain contains two canonical cysteines that are conserved in Ig-like proteins and also has four unique cysteine residues conserved among VISTA orthologs but not present in other B7 family members. The low sequence homology and additional cysteine residues have hindered accurate structural modeling of VISTA based on sequence alone and present a clear need for a high-resolution crystal structure.

Antibodies against VISTA have shown an anti-tumor efficacy in multiple syngeneic mouse models (Liu et al., 2015; Le Mercier et al., 2014; Wang et al., 2011). Therapeutic development has progressed to human clinical trials, with the assessment of a small-molecule antagonist targeting VISTA and PD-L1 (NCT02812875) and the recently terminated trial of an anti-VISTA antibody in patients with advanced cancer (NCT02671955). The purported lead anti-VISTA antibody used in the phase I trial (called "VSTB" here; based on VSTB112) inhibited VISTA signaling *in vitro* and showed tumor regression in a bladder cancer model using human VISTA knockin mice (Snyder et al., 2014); however, little is known about its mechanism of inhibition. Putative regions of interaction between VSTB and VISTA have been proposed, but a specific binding epitope has not been identified. It is also unknown if VSTB can block the VISTA-VSIG3 binding interaction.

We present a high-resolution crystal structure of the human VISTA protein and highlight unique features of the IgV-like fold that distinguish VISTA from other B7 family proteins. We also use combinatorial methods to map the VSTB-VISTA binding epitope and further examine this region for potential VSIG3 interactions. Structural comparisons and epitope analyses performed here provide a blueprint for further VISTA mechanistic research and for the development of next-generation anti-VISTA therapeutics.

RESULTS

Crystallization and Structure Determination of the Extracellular Domain of Human VISTA

The VISTA extracellular domain (ECD) was found to be hyperglycosylated, producing a diffuse protein band that appeared ~15 kDa larger than its predicted molecular mass of ~20 kDa upon analysis by gel electrophoresis (SDS-PAGE). Analysis of the VISTA sequence highlighted five potential locations for N-glycan modification via a NXT/S motif. We mutated three of these asparagine residues (N59, N76, and N158) to glutamine; added Kifunensine, a mannosidase I inhibitor, to the mammalian cell culture media; and treated purified protein with Endo Hf glycosidase prior to crystallization trials. These efforts resulted in an improved discreteness and decreased apparent mass of the purified protein as compared to wild-type (WT) VISTA (Figure S1) and facilitated crystal formation. A complete dataset to 1.85 Å was collected by X-ray diffraction at the Stanford Synchrotron Radiation Lightsource (SSRL) (Table S1). VISTA does not have a suitable template for molecular replacement, as no VISTA homologs are deposited in the PDB, and the closest templates have a sequence identity under 25%. The crystal structure was therefore solved using a combination of molecular replacement (MR), Rosetta modeling, and native sulfur single-wavelength anomalous diffraction (SAD) methods.

The VISTA ECD contains three disulfide bonds, comprising all six cysteine residues found in the VISTA sequence (Figure 1A). The structure consists of 10 beta strands and three alpha helices arranged in a canonical beta-sandwich formation (Figure 1B). The protein is divided into two faces: six beta strands form one coplanar surface, and four beta strands comprise the other. The protein fragment between strands C and C′ comprises 21 residues that form an extended loop and four residues within a predicted alpha helix. An omit map was generated to verify loop density (Figure 1C). The C-C′ loop is stabilized by intramolecular interactions within the loop and with residues from the core of the protein. There are 30 intramolecular hydrogen bonding interactions and a disulfide bond (C51/C113), compared to only four hydrogen bonding interactions with symmetry-related molecules (Figure S2; Table S2). Buried surface area for the interaction of a single monomer with neighboring molecules was found to be only 6.4% of the total monomer surface area. Although these minor interactions with crystal contacts could represent a VISTA-VISTA binding interface on the cell surface, the large number of hydrogen bonds within a single monomer implies that the structure of the C-C′ loop is likely positioned by internal interactions instead of crystal lattice formation. Of the 25 residues in this region, six are positively charged, while only three are negatively charged, creating a net positive charge on this face of the protein (Figure 1D). The structure presented here represents a common Ig-like fold, but as described below, closer examination reveals important differences that make VISTA unique among B7 family proteins.

Structural Comparisons Reveal Deviations of VISTA from the B7 Family

The canonical fold of the B7 family comprises two distinct domains: an IgV domain with nine beta strands and an immunoglobulin constant (IgC) domain with seven beta strands (Collins et al., 2005). Typically, the IgC domain is proximal to the membrane, while the IgV domain is distal and interacts directly with its cognate receptor. Of the seven B7 family proteins that have been crystallized, VISTA is the only family member that lacks an IgC domain. To highlight the structural distinctions of VISTA, we aligned the VISTA ECD with the IgV domain of human PD-L1 (PDB: 4Z18), its closest homolog in the B7 family (23% sequence identity). The overall beta-sandwich fold is evident in both proteins with seven beta strands in VISTA aligning to corresponding strands in the PD-L1 structure (Figure 2A). There are, however, four key differences between VISTA and the classic B7 family fold. First, VISTA contains 10 beta strands, instead of the nine that typically make up an IgV fold. Second, VISTA contains an extra helix (sequence FQDL) in place of a longer beta strand C′ (Figure 2B). This helix is located in the predicted positively charged patch and may constitute a unique epitope that distinguishes VISTA binding interactions from its B7 homologs. Third, VISTA contains the aforementioned 21-residue extended loop (C-C′ loop), which does not align with any B7 family structure (Figure 2C). This region contains seven charged, surface-exposed residues. In comparison, PD-L1 and other B7 family proteins have a significantly smaller, four-residue loop at this location that directly connects two beta strands but does not protrude from the classic beta-sandwich fold. Finally, VISTA contains two additional disulfide bonds (Figure 2D) that are not present in any other B7 family protein but are conserved in VISTA orthologs, including murine and cyno. These two disulfide bonds connect residues C12/C146 and C51/C113, respectively, while the conserved disulfide bond connects beta strands B and F (C22/C114). The uniqueness of the VISTA structure was further corroborated by quantitative comparisons of structural similarity

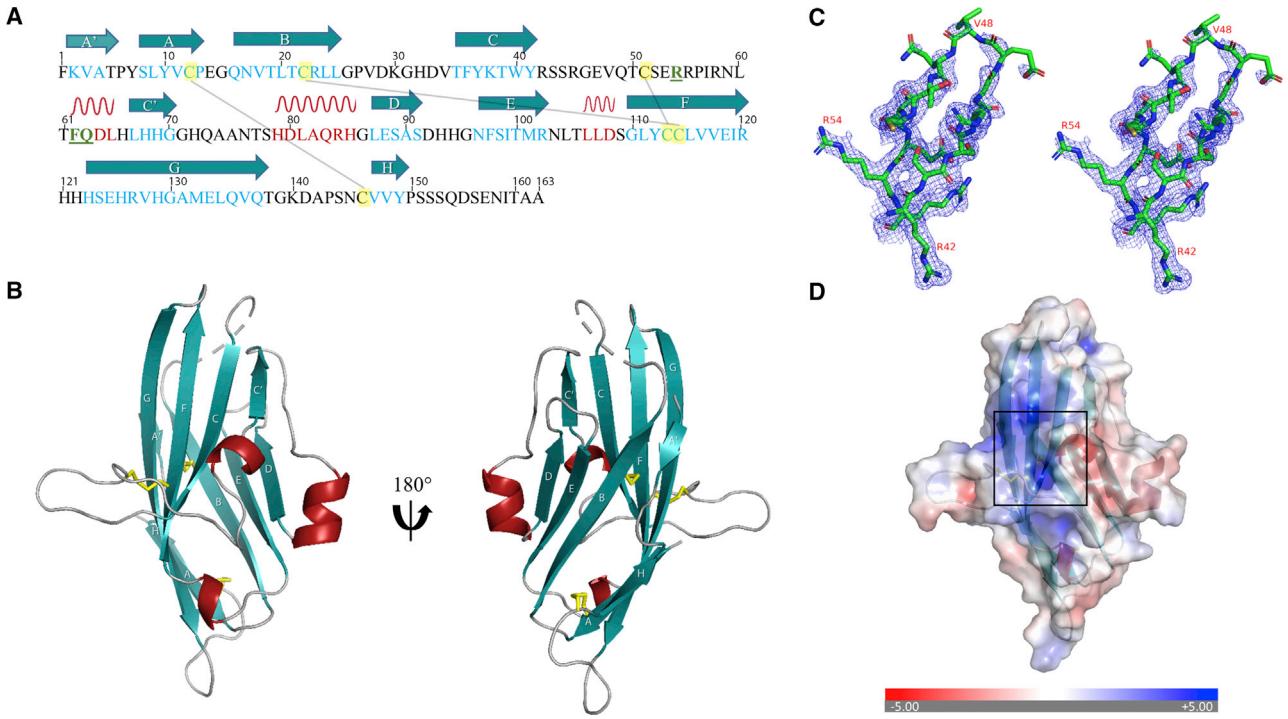

Figure 1. Crystal Structure of Human VISTA

(A) Sequence of human VISTA ECD with labeled secondary structure and cysteines forming disulfide bonds (binding epitope residues: green, underlined).

(B) Cartoon structure of human VISTA ECD colored by secondary structure with beta strands labeled by Ig-domain nomenclature.

(C) Omit map of C-C′ loop.

(D) Electrostatic map of human VISTA (red: negative, blue: positive) revealing the positively charged face of the protein (black square).

See also Figures S1 and S2 and Tables S1 and S2.

with other B7 family proteins. The TM-align server (Zhang and Skolnick, 2005). was used to calculate similarities based on pairwise structural comparisons of known B7 family proteins (Figure 2E). A TM-score above 0.5 predicts proteins of the same fold family, with scores closer to 1.0 indicative of increasingly similar protein structures (Xu and Zhang, 2010). Using these metrics, VISTA is most similar to PD-L1 (0.60) and displays greater structural differences with PD-L2 (0.56), CD80 (0.55), and CD86 (0.56). Notably, all pairwise values for VISTA and other B7 family members are 0.60 or below, whereas pairwise comparisons among all other B7 family members have scores of 0.65 or above. This deviation from the B7 family is not observable by sequence differences alone, as pairwise sequence identities among VISTA and the B7 family members are between 15% and 25%, similar to the bulk of other alignment values (Figure 2E).

Four Residues in the C-C′ Loop Comprise the VSTB-VISTA Binding Epitope

Next, we determined a putative binding epitope of an anti-VISTA antibody VSTB, which is a known inhibitor of VISTA signaling and prevents tumor growth in a human VISTA knockin mouse model of bladder cancer (Snyder et al., 2014). Fine-epitope mapping of VSTB was performed by screening a large library of VISTA mutants displayed on the surface of individual yeast cells to isolate variants that exhibited a loss of antibody binding. Using this method (Chao et al., 2004), we elucidated a set of VISTA residues that mediate VSTB binding. A separate VISTA-binding antibody (referred to as "Ctrl") was tested for conformational and distinct epitope binding to validate the proper folding of VISTA mutants. Heat denaturation of yeast-displayed VISTA followed by incubation with the Ctrl antibody showed a lack of binding, confirming a conformational epitope that depends on VISTA structural integrity (Figure S3A). Additionally, the Ctrl and VSTB antibodies were found to have distinct epitopes through the detection of simultaneous binding of both antibodies (Figure S3B).

A library of VISTA mutants was created via error-prone PCR across the entire gene to achieve, on average, a single amino acid mutation per gene. Yeast were induced for VISTA expression on the cell surface, and iterative rounds of fluorescence-activated cell sorting (FACS) were used to select yeast-displaying VISTA mutants that either lost binding to VSTB ("negative" sort) or retained binding to the Ctrl antibody ("positive" sort) (Figure 3A). Screening using this combination of negative and positive sorting strategies allowed the isolation of residues that directly altered the VSTB binding without disrupting the overall structural integrity of VISTA. In sort 1, the library was incubated with 10 nM of VSTB and screened to isolate VISTA mutants that displayed moderate to negligible binding to VSTB. To increase stringency, yeast collected from sort 1 were subject to a higher concentration of VSTB in sort 2 to isolate VISTA mutants demonstrating even weaker binding to VSTB.

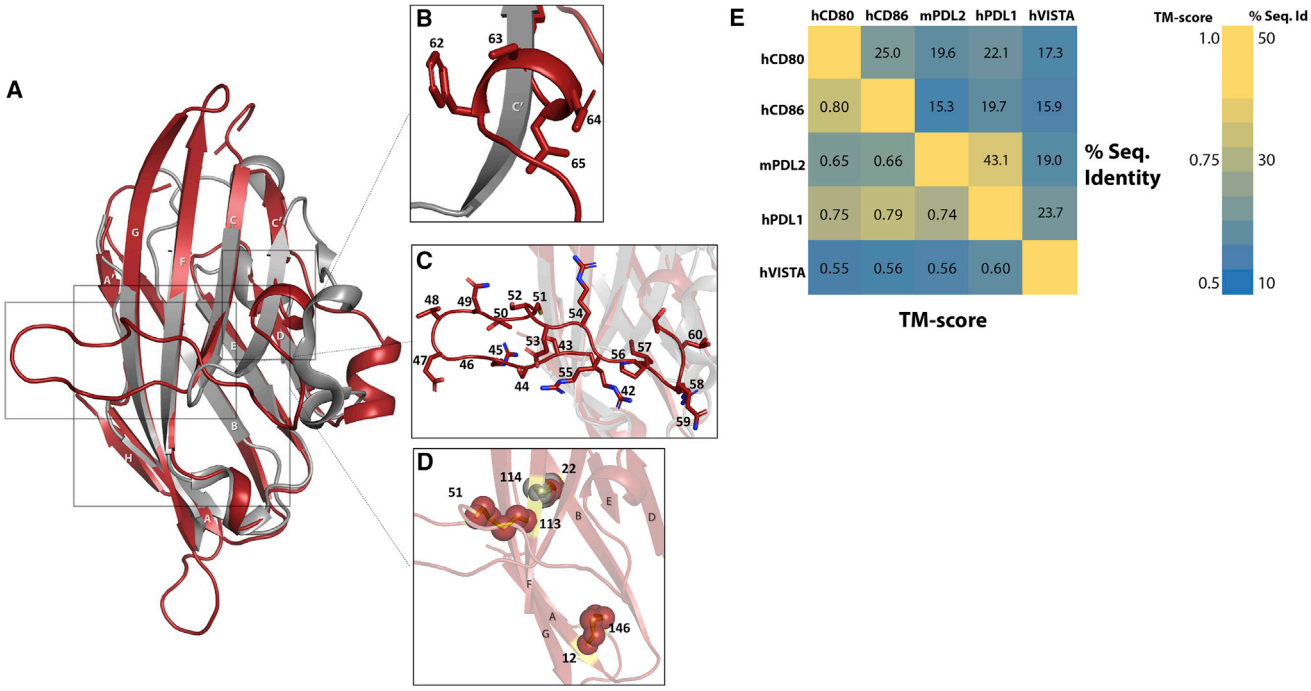

Figure 2. Structural Deviations of VISTA from the B7 Family

(A) Cartoon structure of the human VISTA ECD (red) aligned with the IgV domain of human PD-L1 (gray).

(B) Unique helix in VISTA in place of beta strand in PD-L1.

(C) Unique C-C′ loop in VISTA that extends from the beta-sandwich core.

(D) Disulfide bonds in VISTA (red spheres, yellow residues), including two unique disulfides (red spheres) in addition to conserved disulfide bond (C22, C114) between strands B and F (gray spheres).

(E) Heatmap of pairwise TM-scores (bottom-left half) and sequence identities (top-right half) between human VISTA (hVISTA) and the IgV domains of four other B7 family proteins.

A VSTB-negative binding population was clearly enriched in sort 2 (25.2% in gate) compared to the small number of negative clones observed in sort 1 (3.4% in gate). In sort 3, 50 nM of the Ctrl antibody (about 200× the apparent K_d) was used to isolate yeast-displayed VISTA mutants that retained structural integrity to bind the Ctrl antibody. The screening stringency was again increased in sort 4 by using an even higher concentration of VSTB (200 nM) to select for mutations that almost completely decreased antibody binding. By sort 4, close to 70% of the yeast-displayed VISTA clones showed weak to negative binding to VSTB. The remaining yeast clones were subject to a final positive sort using a lower concentration of Ctrl (about 20× the apparent K_d) to further confirm the retention of VISTA structural integrity.

Following the library screening, 50 yeast clones were randomly selected for sequencing analysis to help identify a subset of residues directly involved in VSTB binding. Five mutations appeared in multiple (>4) sequenced clones: F62L, R54C, S124P, Q63R, and R58G (Table S3). All identified residues, with the exception of S124P, were localized to the alpha helix and extended loop fragment that is unique to the VISTA structure (Figure 3B). Each residue was then individually mutated to alanine via site-directed mutagenesis to confirm that the residue locations, as opposed to the specific amino acid mutations, were drivers of VSTB binding. The binding of S124A to VSTB appeared to be equivalent to that of the WT VISTA binding to VSTB (Figure S3C), suggesting that the proline mutation in S124P indirectly affected VSTB binding by modifying the local fold of the VISTA protein. This mutant was therefore excluded from the proposed epitope and was not subject to further analysis. In contrast, the remaining four mutants (R54A, R58A, F62A, and Q63A) were each found to individually affect binding to VSTB (Figure 3C). Binding signal generated from 250 nM of VSTB clearly shows weak binding of the F62A and Q63A mutants and almost no detectable binding of the R54A and R58A mutants, demonstrating that these four residues are critical for VISTA binding to VSTB (Figure 3D).

Because of the proximity of these mapped residues to the N59 genetically modified glycan site (Figure S4A), we measured the binding of VSTB to WT VISTA or the triple N59Q/N76Q/N158Q mutant used for crystallization (Figure S4B), and no significant differences were observed (apparent K_d values of ~0.9 nM). Additionally, the N59 residue appears to be solvent exposed and points away from the internal hydrophobic core; therefore, glycosylation at this location is unlikely to affect loop structure (Figure S4C). A valid epitope must also be surface exposed to allow for unhindered interactions with antibodies and other binding proteins. Residues R54, F62, and Q63 have exposures above

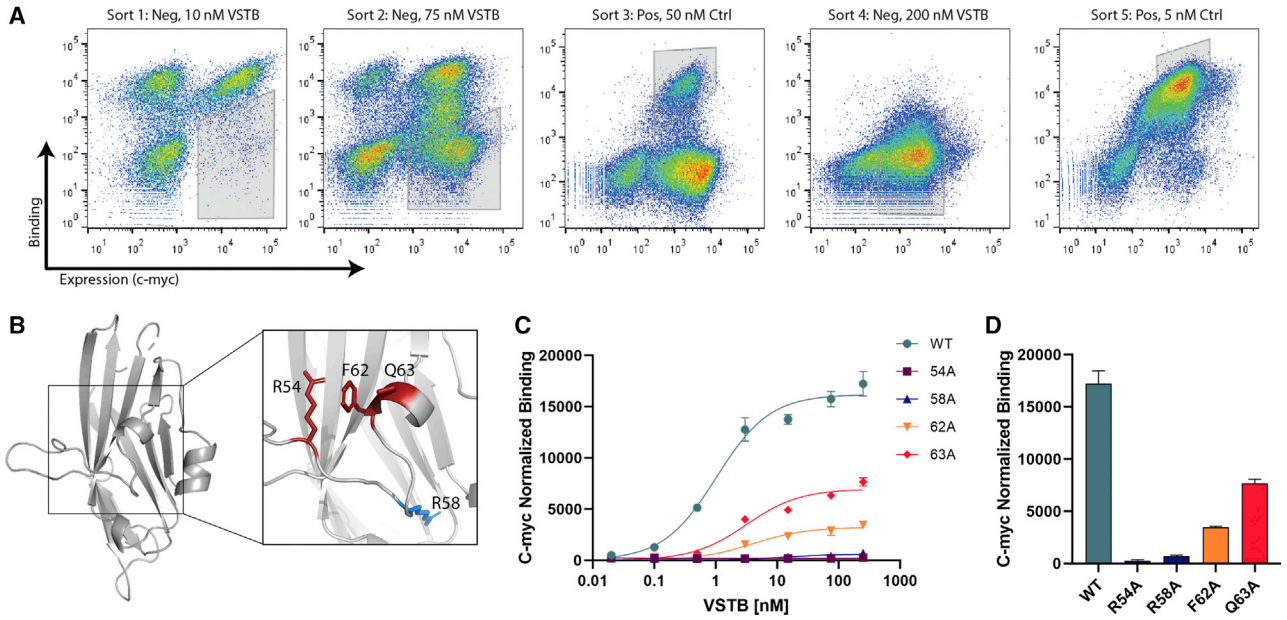

Figure 3. Mapping the VSTB Binding Epitope of VISTA

(A) Library screening progression used to isolate yeast-displayed VISTA mutants that retained or reduced antibody binding. FACS gates are shown in gray boxes on dot plots of individual positive or negative sorts.

(B) Residues identified from epitope mapping highlighted in red on the human VISTA ECD structure. R58 (blue) was excluded from defining the VSTB epitope due to its lower surface exposure and involvement with hydrophobic packing and intramolecular interactions

(C) Binding of the soluble VSTB antibody to yeast-displayed human VISTA with single amino acid alanine substitutions. Means ± standard deviation for duplicate measurements are shown in (C) and (D).

(D) Binding signal comparison of 250 nM of VSTB to yeast-displayed hVISTA alanine mutants.

See also Figures S3 and S4 and Table S3.

35%, while the R58 residue has a lower exposure of 23%, consistent with its internal-facing side chain. All four residues have significantly greater accessible areas than fully buried residues (e.g., solvent accessibilities for the buried W40 and F97 residues are <1%). Further analysis of intramolecular interactions revealed R58 as integral to the local C-C′ loop structure due to its extensive involvement with hydrophobic packing and intramolecular interactions (Figure S4C). Therefore, R58 likely stabilizes a local loop turn, and mutations at this location would disrupt the folding of surrounding residues. Based on this analysis, R58 appears to have been highlighted as an artifact of the screening process and was therefore excluded from further analysis as an epitope residue.

VISTA Interacts with VSIG3 via a Shared VSTB Binding Epitope

The VSTB antibody has been shown to inhibit VISTA signaling; thus, the residues we identified above suggest a functional epitope through which to guide future drug discovery efforts. Since the epitope for the recently proposed VISTA ligand VSIG3 is unknown, we tested whether VSTB operates through direct ligand competition of VSIG3 at the residues mapped above and demonstrate an overlap of the purported VSTB binding epitope with the VISTA-VSIG3 interaction.

WT VISTA and a VISTA triple mutant containing the R54A, F62A, and Q63A mutations were solubly expressed in mammalian cells. To confirm the structural integrity of the triple mutant, the Ctrl antibody was first tested for binding to WT VISTA or the 54A/62A/63A triple mutant using an ELISA-based assay. Binding to the Ctrl antibody was retained for the 54A/62A/63A triple mutant with no significant difference in binding from WT VISTA in any concentration tested (Figure 4A). In contrast, the three mutations significantly diminish binding to VSTB at every concentration tested (>95% decrease compared to WT VISTA). The R54A, F62A, and Q63A mutations therefore abrogate binding to VSTB but do not alter the VISTA structure significantly to abolish binding to the Ctrl antibody. A binding assay was then performed between the VSIG3 ligand and the triple mutant or WT VISTA (Figure 4B). WT VISTA bound to VSIG3 with an apparent K_d of ~2 μM, while the triple mutant bound with a significantly weaker apparent K_d of >20 μM, indicating that VISTA binding to VSIG3 is highly dependent on three of the same mutations that comprise the VSTB binding epitope. To further confirm the shared epitope, we pre-complexed WT VISTA with varying concentrations of VSTB and measured the binding to VSIG3 (Figure 4C). Dose-response disruption of VSIG3 binding is evident, with concentrations above 500 nM of VSTB completely abolishing the VISTA-VSIG3 interaction. The 54A/62A/63A VISTA mutant and pre-complexed VISTA/VSTB have significantly lower VSIG3 binding than WT VISTA or pre-complexed VISTA-isotype control (Figure 4D). This analysis suggests that the mapped VISTA epitope is not only important for interaction with an antibody that has been

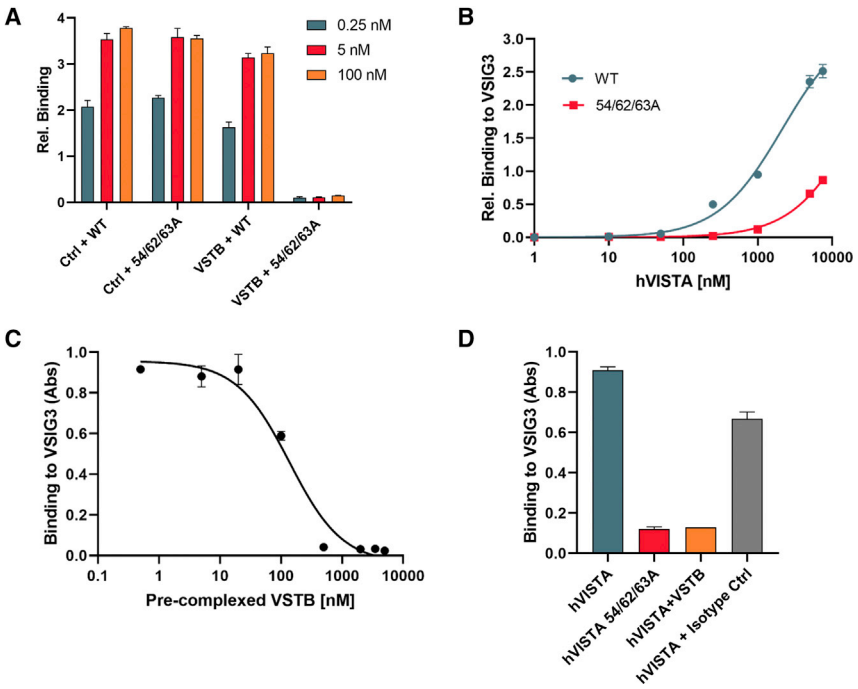

Figure 4. VSIG3 Interacts with VISTA via the VSTB Binding Epitope

(A) Binding of WT or VISTA 54A/62A/63A to the Ctrl or VSTB antibody in an ELISA format. VISTA was added to well-coated antibody at three different concentrations.

(B) An ELISA binding assay with well-coated VSIG3 incubated with soluble WT or VISTA 52A/62A/63A.

(C) Competition binding of 1 μM WT VISTA, pre-complexed with a range of VSTB concentrations, to well-coated VSIG3 in an ELISA format.

(D) VSIG3 binding signal comparison of 1 μM WT VISTA, 1 μM VISTA 54A/62A/63A, 1 μM VISTA pre-complexed with 500 nM of VSTB, and 1 μM VISTA pre-complexed with 500 nM IgG isotype control.

Means ± SD for triplicate measurements are shown.

shown to inhibit VISTA signaling, but also underlies binding to VSIG3, a known functional partner of VISTA.

DISCUSSION

In this work, we determined a high-resolution structure of VISTA facilitated by protein deglycosylation strategies and a combinatorial MR-Rosetta pipeline used to obtain the final structure. A combination of genetic mutations (N → Q) in the VISTA sequence, a glycosylation inhibitor added to the mammalian cell culture media, and enzymatic deglycosylation post-purification was required to produce VISTA at its expected molecular mass. Previous crystallization attempts from our group using WT VISTA or Endo Hf-treated VISTA without genetic mutations were not successful, highlighting the importance of these steps for crystal growth. Additionally, solving the structure required modeling efforts via Rosetta and an iterative pipeline of structure refinement and molecular replacement. In particular, the unique loop and helix regions do not fit the classic Ig-like fold and thus could not be solved with molecular replacement alone. We foresee the strategy described here and the PDB-deposited VISTA coordinates assisting future efforts in solving difficult Ig-like protein structures.

A combinatorial strategy for fine-epitope mapping was used to isolate an epitope important for binding to VSTB, an anti-VISTA antibody of therapeutic interest, and this information in turn was used to determine a proposed overlapping epitope for the VSIG3 ligand. Previously, hydrogen-deuterium exchange was used to highlight a number of potential binding hotpots of VSTB to VISTA (Snyder et al., 2014). In our work, we provide clarity on this important region of interaction and corroborate the relevance of this epitope for VISTA function. We recognize that the yeast-display-based epitope mapping approach used here may not elucidate every region involved in binding and can be limited or confounded by residues that drive allosteric changes, residues whose glycosylation patterns differ among yeast and mammals, residues that affect VISTA expression but are part of the VSTB binding interface, or residues that are shared between the VSTB and Ctrl epitopes. In this work, several factors provide confidence that our approach has identified the critical binding epitope driving the VISTA/VSTB interaction. WT VISTA and the N → Q VISTA variant bind to VSTB with similar affinities, which minimizes the impact of differential glycosylation of yeast-surface-displayed proteins. In addition, the three epitope residues identified form a solvent exposed, contiguous surface. Finally, when mutated to alanine, each isolated residue disrupts VSTB binding on yeast, while the three mutations together completely abrogate VSTB binding, as measured by ELISA.

VSIG3 was only recently discovered by ELISA-based binding screens as a purported cognate binding partner for VISTA expressed on T cells (Wang et al., 2019; Yang et al., 2017). Here, we build on this evidence by confirming ELISA-based binding of VSIG3 to VISTA and show that the inhibitory antibody VSTB blocks this specific interaction. Although there may be other VISTA binding partners, and inhibitory antibodies may partially function through an induced allosteric change of VISTA, we hypothesize that the reported inhibitory function of the VSTB antibody is at least partly due to its blocking of the VSIG3-VISTA binding, analogous to anti-PD-1 antibodies blocking the PD-1/PD-L1 signaling axis (Sznol and Chen, 2013). Future experiments using antibodies that bind VISTA but do not block VISTA-VSIG3 binding are needed to confirm the importance of this signaling axis for anti-VISTA immunotherapy. We demonstrate that the three isolated VISTA residues (R54, F62, and Q63) at least partially drive VSIG3 binding but recognize that additional information would be necessary to completely define this interaction. Fine-epitope mapping of the VSIG3-VISTA interaction using a yeast-display method could not be performed due to the lack

of a robust binding signal detected on yeast, likely due to its weak affinity. In addition, attempts to crystallize the VSIG3-VISTA co-complex were unsuccessful.

Comparing the structure of VISTA to PD-L1 reveals important qualities that diverge from the B7 protein family. The non-canonical and conserved C51/C113 disulfide bond is unique to the VISTA structure and likely stabilizes the protrusion of the extended C-C′ loop outward from the beta-sandwich core. Additionally, VISTA contains a singular IgV-like domain, while all other B7 family members contain both an IgV and an IgC domain. The B7 family members B7-1 (CD80), B7-2 (CD86), B7-DC (PD-L2), B7-H1 (PD-L1), and B7-H3 (CD276) are all dual-domain proteins, and all function primarily as ligands. In contrast, the cognate receptors of these proteins, including CD28, CTLA-4, ICOS, and PD-1, all have single IgV domain structures. Based on its domain composition and its binding interaction with VSIG3, VISTA appears to be more similar in architecture and function with the receptors than with the B7 family ligands.

Knowledge of the three-dimensional structure of VISTA and residues that comprise its binding epitope can help guide future drug development by enabling small-molecule library screening through computer-aided drug design (CADD) (Yu and MacKerell, 2017) and computational antibody screens through antibody-antigen docking (Kilambi and Gray, 2017; Weitzner et al., 2017). Additionally, the high-resolution structure can support future studies of receptor or ligand interactions through computational docking experiments. The coordinates for the VISTA ECD will also expedite co-crystallization efforts of VISTA complexes by providing a well-suited template for molecular replacement. The initial success of checkpoint inhibitors in the clinic has provided a blueprint for new drugs that release the breaks on the immune system. VISTA inhibitors have the potential to provide an orthogonal method of T cell stimulation and anti-tumor activity by directly affecting the antigen-presenting cell (APC)/T cell signaling axis. We believe the high-resolution crystal structure of VISTA presented here will bolster these efforts by encouraging further VISTA-related research and by directly assisting drug development endeavors.

STAR★METHODS

Detailed methods are provided in the online version of this paper and include the following:

- KEY RESOURCES TABLE
- LEAD CONTACT AND MATERIALS AVAILABILITY
- EXPERIMENTAL MODEL AND SUBJECT DETAILS
- METHOD DETAILS
  - Preparation of recombinant VISTA protein
  - Crystallization and data collection
  - Structure determination and refinement
  - Structural comparisons, electrostatic surfaces, solvent accessibility, and buried surface area
  - Epitope mapping
  - Binding assays
- QUANTIFICATION AND STATISTICAL ANALYSIS
- DATA AND CODE AVAILABILITY

SUPPLEMENTAL INFORMATION

Supplemental Information can be found online at https://doi.org/10.1016/j.celrep.2019.07.073.

ACKNOWLEDGMENTS

The authors thank Daniel Fernandez for crystallization assistance and advice, Ryan Kelly for providing materials and advice used in epitope mapping, Qingping Xu for providing the script used for automated MR search, Jenifer Brown and Lindsay Deis for initial crystallization attempts and assistance, Sean Hunter and James Kintzing for helpful discussions regarding manuscript preparation, Jun Kim for providing helpful protein de-glycosylation strategies, the Stanford FACS Core Facility for assistance with flow cytometric sorting, and the ChEM-H Macromolecular Structure Knowledge Center (MSKC) for assistance with crystal screening. Portions of this research were performed at the Stanford Synchrotron Radiation Laboratory, a national user facility operated by Stanford University on behalf of the U.S. Department of Energy, Office of Science, and Office of Basic Energy Sciences under contract DE-AC02-76SF00515. The SSRL Structural Molecular Biology Program is supported by the DOE Office of Biological and Environmental Research and by the NIH National Institute of General Medical Sciences (including P41GM103393). This work was supported by the Stanford Bio-X IIP Interdisciplinary Initiatives Seed Grants Program (J.R.C.), NSF Graduate Research Fellowship (N.M.), Stanford Graduate Fellowship (N.M.), Stanford Bio-X Undergraduate Summer Research Program (S.M.), and Stanford NIST Predoctoral Training Grant Program (R.A.P.S.).

AUTHOR CONTRIBUTIONS

N.M. and S.M. performed the protein preparation and initial crystallization attempts. I.I.M. performed the crystallization optimization and X-ray diffraction. P.-S.H. and I.I.M. performed the structure refinement and determination. R.A.P.S. carried out homology modeling. N.M. and S.M. completed epitope mapping, and N.M. performed single clone analysis and functional epitope experiments. N.M. analyzed the data. N.M. and J.R.C. prepared the manuscript with input from all coauthors.

DECLARATION OF INTERESTS

J.R.C. is a co-founder, director, and stockholder in xCella Biosciences, which is developing antibody therapeutics for applications in oncology. N.M. is a co-inventor on intellectual property related to work on VISTA. Other authors declare no competing financial interests.

Received: April 12, 2019
Revised: June 13, 2019
Accepted: July 19, 2019
Published: September 3, 2019

REFERENCES

Adams, P.D., Afonine, P.V., Bunkóczi, G., Chen, V.B., Davis, I.W., Echols, N., Headd, J.J., Hung, L.-W., Kapral, G.J., Grosse-Kunstleve, R.W., et al. (2010). PHENIX: a comprehensive Python-based system for macromolecular structure solution. Acta Crystallogr. D Biol. Crystallogr. *66*, 213–221.

Boder, E.T., and Wittrup, K.D. (1997). Yeast surface display for screening combinatorial polypeptide libraries. Nat. Biotechnol. *15*, 553–557.

Boder, E.T., and Wittrup, K.D. (2000). Yeast surface display for directed evolution of protein expression, affinity, and stability. Methods Enzymol. *328*, 430–444.

Chao, G., Cochran, J.R., and Wittrup, K.D. (2004). Fine epitope mapping of anti-epidermal growth factor receptor antibodies through random mutagenesis and yeast surface display. J. Mol. Biol. *342*, 539–550.

Chao, G., Lau, W.L., Hackel, B.J., Sazinsky, S.L., Lippow, S.M., and Wittrup, K.D. (2006). Isolating and engineering human antibodies using yeast surface display. Nat. Protoc. *1*, 755–768.

Cho, B.K., Kieke, M.C., Boder, E.T., Wittrup, K.D., and Kranz, D.M. (1998). A yeast surface display system for the discovery of ligands that trigger cell activation. J. Immunol. Methods *220*, 179–188.

Colby, D.W., Kellogg, B.A., Graff, C.P., Yeung, Y.A., Swers, J.S., and Wittrup, K.D. (2004). Engineering antibody affinity by yeast surface display. Methods Enzymol. *388*, 348–358.

Collins, M., Ling, V., and Carreno, B.M. (2005). The B7 family of immune-regulatory ligands. Genome Biol. *6*, 223.

Cowtan, K., Main, P., and Cr, I.U. (1998). Miscellaneous algorithms for density modification. Acta Crystallogr. Sect. D Biol. Crystallogr. *54*, 487–493.

Dolinsky, T.J., Czodrowski, P., Li, H., Nielsen, J.E., Jensen, J.H., Klebe, G., and Baker, N.A. (2007). PDB2PQR: expanding and upgrading automated preparation of biomolecular structures for molecular simulations. Nucleic Acids Res. *35*, W522–W525.

Emsley, P., and Cowtan, K. (2004). Coot: model-building tools for molecular graphics. Acta. Crystallogr. Sect. D. Biol. Crystallogr. *60*, 2126–2132.

Flies, D.B., Han, X., Higuchi, T., Zheng, L., Sun, J., Ye, J.J., and Chen, L. (2014). Coinhibitory receptor PD-1H preferentially suppresses $CD4^+$ T cell-mediated immunity. J. Clin. Invest. *124*, 1966–1975.

Flies, D.B., Higuchi, T., and Chen, L. (2015). Mechanistic assessment of PD-1H coinhibitory receptor-induced T cell tolerance to allogeneic antigens. J. Immunol. *194*, 5294–5304.

Gao, J., Ward, J.F., Pettaway, C.A., Shi, L.Z., Subudhi, S.K., Vence, L.M., Zhao, H., Chen, J., Chen, H., Efstathiou, E., et al. (2017). VISTA is an inhibitory immune checkpoint that is increased after ipilimumab therapy in patients with prostate cancer. Nat. Med. *23*, 551–555.

Huang, P.-S., Ban, Y.-E.A., Richter, F., Andre, I., Vernon, R., Schief, W.R., and Baker, D. (2011). RosettaRemodel: A Generalized Framework for Flexible Backbone Protein Design. PLoS One *6*, e24109.

Jurrus, E., Engel, D., Star, K., Monson, K., Brandi, J., Felberg, L.E., Brookes, D.H., Wilson, L., Chen, J., Liles, K., et al. (2018). Improvements to the APBS biomolecular solvation software suite. Protein Sci. *27*, 112–128.

Kabsch, W. (2010). XDS. Acta Crystallogr. D Biol. Crystallogr. *66*, 125–132.

Kakavand, H., Jackett, L.A., Menzies, A.M., Gide, T.N., Carlino, M.S., Saw, R.P.M., Thompson, J.F., Wilmott, J.S., Long, G.V., and Scolyer, R.A. (2017). Negative immune checkpoint regulation by VISTA: a mechanism of acquired resistance to anti-PD-1 therapy in metastatic melanoma patients. Mod. Pathol. *30*, 1666–1676.

Kilambi, K.P., and Gray, J.J. (2017). Structure-based cross-docking analysis of antibody-antigen interactions. Sci. Rep. *7*, 8145.

Krissinel, E., and Henrick, K. (2007). Inference of macromolecular assemblies from crystalline state. J. Mol. Biol. *372*, 774–797.

Le Mercier, I., Chen, W., Lines, J.L., Day, M., Li, J., Sergent, P., Noelle, R.J., and Wang, L. (2014). VISTA regulates the development of Protective antitumor immunity. Cancer Res. *74*, 1933–1944.

Lee, B., and Richards, F.M. (1971). The interpretation of protein structures: estimation of static accessibility. J. Mol. Biol. *55*, 379–400.

Lines, J.L., Pantazi, E., Mak, J., Sempere, L.F., Wang, L., O'Connell, S., Ceeraz, S., Suriawinata, A.A., Yan, S., Ernstoff, M.S., and Noelle, R. (2014). VISTA is an immune checkpoint molecule for human T cells. Cancer Res. *74*, 1924–1932.

Liu, J., Yuan, Y., Chen, W., Putra, J., Suriawinata, A.A., Schenk, A.D., Miller, H.E., Guleria, I., Barth, R.J., Huang, Y.H., and Wang, L. (2015). Immune-checkpoint proteins VISTA and PD-1 nonredundantly regulate murine T-cell responses. Proc. Natl. Acad. Sci. USA *112*, 6682–6687.

Liu, J., Xie, X., Xuan, C., Li, T., Wang, L., Teng, L., and Liu, J. (2018). High-density infiltration of V-domain immunoglobulin suppressor of T-cell activation up-regulated immune cells in human pancreatic cancer. Pancreas *47*, 725–731.

McCoy, A.J., Grosse-Kunstleve, R.W., Adams, P.D., Winn, M.D., Storoni, L.C., and Read, R.J. (2007). Phaser crystallographic software. J. Appl. Cryst. *40*, 658–674.

Mulati, K., Hamanishi, J., Matsumura, N., Chamoto, K., Mise, N., Abiko, K., Baba, T., Yamaguchi, K., Horikawa, N., Murakami, R., et al. (2019). VISTA expressed in tumour cells regulates T cell function. Br. J. Cancer *120*, 115–127.

Snyder, L., Powers, G., Sepulveda, M.A., and Alvarez, J. (2014). Anti-vista antibodies and fragments, Janssen Pharmaceuticals Patent WO2016207717.

Song, Y., DiMaio, F., Wang, R.Y.-R., Kim, D., Miles, C., Brunette, T., Thompson, J., and Baker, D. (2013). High-resolution comparative modeling with RosettaCM. Structure *21*, 1735–1742.

Sznol, M., and Chen, L. (2013). Antagonist antibodies to PD-1 and B7-H1 (PD-L1) in the treatment of advanced human cancer. Clin. Cancer Res. *19*, 1021–1034.

Terwilliger, T.C., Dimaio, F., Read, R.J., Baker, D., Bunkóczi, G., Adams, P.D., Grosse-Kunstleve, R.W., Afonine, P.V., and Echols, N. (2012). phenix.mr_rosetta: molecular replacement and model rebuilding with Phenix and Rosetta. J. Struct. Funct. Genomics *13*, 81–90.

Van Deventer, J.A., and Wittrup, K.D. (2014). Yeast surface display for antibody isolation: library construction, library screening, and affinity maturation. In Monoclonal Antibodies: Methods and Protocols, V. Ossipow and N. Fischer, eds. (Humana Press), pp. 151–181.

Villarroel-Espindola, F., Yu, X., Datar, I., Mani, N., Sanmamed, M., Velcheti, V., Syrigos, K., Toki, M., Zhao, H., Chen, L., et al. (2018). Spatially resolved and quantitative analysis of VISTA/PD-1H as a novel immunotherapy target in human non–small cell lung cancer. Clin. Cancer Res. *24*, 1562–1573.

Wang, W., and Malcolm, B.A. (1999). Two-stage PCR protocol allowing introduction of multiple mutations, deletions and insertions using QuikChange Site-Directed Mutagenesis. Biotechniques *26*, 680–682.

Wang, L., Rubinstein, R., Lines, J.L., Wasiuk, A., Ahonen, C., Guo, Y., Lu, L.-F., Gondek, D., Wang, Y., Fava, R.A., et al. (2011). VISTA, a novel mouse Ig superfamily ligand that negatively regulates T cell responses. J. Exp. Med. *208*, 577–592.

Wang, L., Jia, B., Claxton, D.F., Ehmann, W.C., Rybka, W.B., Mineishi, S., Naik, S., Khawaja, M.R., Sivik, J., Han, J., et al. (2018). VISTA is highly expressed on MDSCs and mediates an inhibition of T cell response in patients with AML. OncoImmunology *7*, e1469594.

Wang, J., Wu, G., Manick, B., Hernandez, V., Renelt, M., Erickson, C., Guan, J., Singh, R., Rollins, S., Solorz, A., et al. (2019). VSIG-3 as a ligand of VISTA inhibits human T-cell function. Immunology *156*, 74–85.

Weitzner, B.D., Jeliazkov, J.R., Lyskov, S., Marze, N., Kuroda, D., Frick, R., Adolf-Bryfogle, J., Biswas, N., Dunbrack, R.L., Jr., and Gray, J.J. (2017). Modeling and docking of antibody structures with Rosetta. Nat. Protoc. *12*, 401–416.

Xie, S., Huang, J., Qiao, Q., Zang, W., Hong, S., Tan, H., Dong, C., Yang, Z., and Ni, L. (2018). Expression of the inhibitory B7 family molecule VISTA in human colorectal carcinoma tumors. Cancer Immunol. Immunother. *67*, 1685–1694.

Xu, J., and Zhang, Y. (2010). How significant is a protein structure similarity with TM-score = 0.5? Bioinformatics *26*, 889–895.

Yang, W., Padkjær, S.B., Wang, J., Sun, Z., Shan, B., Yang, L., Chen, H., Kang, L., Madsen, D., Li, X., et al. (2017). Construction of a versatile expression library for all human single-pass transmembrane proteins for receptor pairings by high throughput screening. J. Biotechnol. *260*, 18–30.

Yu, W., and MacKerell, A.D., Jr. (2017). Computer-aided drug design methods. Methods Mol. Biol. *1520*, 85–106.

Zhang, Y., and Skolnick, J. (2005). TM-align: a protein structure alignment algorithm based on the TM-score. Nucleic Acids Res. *33*, 2302–2309.

STAR★METHODS

KEY RESOURCES TABLE

REAGENT or RESOURCE	SOURCE	IDENTIFIER
Antibodies		
chicken anti-c-myc	Invitrogen	Cat# A21281, RRID: AB_2535826
anti-mouse IgG, Alexa Fluor 488	Thermo Fisher Scientific	Cat# A-11059, RRID: AB_2534106
anti-human IgG, Alexa Fluor 647	Thermo Fisher Scientific	Cat# A-21445, RRID: AB_2535862
rabbit anti-6-HIS, FITC	Bethyl	Cat# A190-114F, RRID: AB_1944199
goat anti-rabbit IgG HRP	Novus Biologicals	Cat# NB7160, RRID: AB_524669
anti-chicken IgY (H+L), Alexa Fluor 647	abcam	ab150171
anti-chicken IgY (H+L), Alexa Fluor 488	Thermo Fisher Scientific	Cat# A11039, RRID: AB_2534096
Chemicals, Peptides, and Recombinant Proteins		
VSTB Antibody	VSTB112 Sequence (Snyder et al., 2014)	N/A
Ctrl Antibody	Gift from xCella Biosciences	N/A
human VISTA-HIS	This paper	N/A
human VSIG3-Fc	R&D Systems	9229-VS-050
HEPES sodium salt	Sigma	H7006
Sodium Chloride (NaCl)	Sigma-Aldrich	S3014
Sodium Bromide (NaBr)	Sigma-Aldrich	229881
Polyethylene glycol 3350	Spectrum	PO125
1M Tris-HCl (pH 8.0)	Sigma-Aldrich	T2694
ADA	Sigma	00307
Critical Commercial Assays		
Seed Bead Kit	Hampton Research	HR2-320
Expi293 Transfection Kit	GIBCO	A14525
Deposited Data		
human VISTA ECD X-ray structure	This paper	PDB: 6OIL
Experimental Models: Cell Lines		
Expi293 HEKs	GIBCO	A14635
Experimental Models: Organisms/Strains		
DH10B E. Coli	Invitrogen	18290015
EBY100 Yeast	ATCC	MYA-4941
Oligonucleotides		
GTACAGACGTGTTCAGAGGCCCGACCTATCA GGCAGCTT	This paper	hVISTA SDM 54A_Fwd (169)
AAGCTGCCTGATAGGTCGGGCCTCTGAACAC GTCTGTAC	This paper	hVISTA SDM 54A_Rev (170)
TCAGAGCGCCGACCTATCGCCCAGCTTACG TTTCAGGAT	This paper	hVISTA SDM 58A_Fwd (171)
ATCCTGAAACGTAAGCTGGGCGATAGGTCGG CGCTCTGA	This paper	hVISTA SDM 58A_Rev (172)
CCTATCAGGCAGCTTACGGCCCAGGATCTGC ATCTTCAC	This paper	hVISTA SDM 62A_Fwd (173):
GTGAAGATGCAGATCCTGGGCCGTAAGCTGC CTGATAGG	This paper	hVISTA SDM 62A_Rev (174)
ATCAGGCAGCTTACGTTTGCCGATCTGCATC TTCACCAC	This paper	hVISTA SDM 63A_Fwd (175)
GTGGTGAAGATGCAGATCGGCAAACGTAAGC TGCCTGAT	This paper	hVISTA SDM 63A_Rev (176)

(*Continued on next page*)

Continued

REAGENT or RESOURCE	SOURCE	IDENTIFIER
GAAATACGCCACCACCATGCCGAACATAGAG TACATGGA	This paper	hVISTA SDM 124A_Fwd (177)
TCCATGTACTCTATGTTCGGCATGGTGGTGGC GTATTTC	This paper	hVISTA SDM 124A_Rev (178)
Recombinant DNA		
pAdd2-VISTA-6xHIS	This paper	N/A
pCTCon2-hVISTA-NQ	This paper	N/A
pCTCon2-hVISTA-WT	This paper	N/A
pCTCon2-hVISTA Alanine Mutants	This paper	N/A
pCTCon2-mVISTA	This paper	N/A
pCTCon2 yeast surface expression plasmid	Gift from Dane Wittrup lab	N/A
Software and Algorithms		
Rosetta	RosettaCommons	https://www.rosettacommons.org/software/license-and-download
Phaser	McCoy et al., 2007	N/A
Phenix	Adams et al., 2010	https://www.phenix-online.org/
Buccaneer	Cowtan et al., 1998	N/A
Coot	Emsley and Cowtan, 2004	https://www2.mrc-lmb.cam.ac.uk/personal/pemsley/coot/
Pymol	The PyMOL Molecular Graphics System, Version 2.3 Schrödinger, LLC	https://pymol.org/2/
PISA	Krissinel and Henrick, 2007	https://www.ebi.ac.uk/pdbe/pisa/
AreaImol	Lee and Richards, 1971	http://www.ccp4.ac.uk/html/areaimol.html
RosettaCM	Song et al., 2013	N/A
RosettaRemodel	Huang et al., 2011	N/A
Phenix-rosetta	Terwilliger et al., 2012	N/A

LEAD CONTACT AND MATERIALS AVAILABILITY

Further information and requests for resources and reagents should be directed to and will be fulfilled by the Lead Contact, Jennifer Cochran (cochran1@stanford.edu). This study did not generate new unique reagents.

EXPERIMENTAL MODEL AND SUBJECT DETAILS

Expi293F cells were acquired from ThermoFisher Scientific and grown in Expi293 Expression Medium according to the manufacturer's protocol. DH10B *E. coli* cells were grown in Luria-Bertani (LB) media at 37°C shaking at 250 revolutions per minute (RPM). EBY100 yeast were grown according to previously published protocols (Van Deventer and Wittrup, 2014). Briefly, yeast were grown in minimal media with dextrose (SD-CAA) at 30°C shaking at 235 RPM and induced for surface expression in minimal media with galactose (SG-CAA) at 20°C shaking at 235 RPM.

METHOD DETAILS

Preparation of recombinant VISTA protein

The human VISTA extracellular domain (ECD) sequence with native signal peptide (Met1-Ala194, UniProt) was ordered as a gblock Gene Fragment (IDT) and cloned into the cytomegalovirus-driven adenoviral shuttle vector pAdd2 with a C-terminal 6x HIS-tag using standard Gibson cloning at EcoRI/XhoI vector cut sites. Protein was expressed in Expi293 cells according to the manufacturer's protocol, and proteins were purified from culture supernatant using nickel affinity chromatography. An hVISTA triple mutant (R54A, F62A, Q63A) used for epitope binding verification was produced in a similar manner. For crystallization, an asparagine triple mutant (N59Q, N76Q, N158Q) was cloned into the pAdd2 expression plasmid as described above and expressed in Expi293 cells in the presence of 10 μM Kifunensine (Cayman Chemical, 109944-15-2). After nickel affinity chromatography, N-linked glycans were removed using

endoglycosidase H (Endo Hf, New England BioLabs, P0703). De-glycosylated VISTA protein was separated from Endo Hf via additional nickel affinity chromatography. Residues are numbered starting after the signal peptide (Phe1, Lys2, Val3).

Crystallization and data collection

VISTA ECD protein was concentrated to 8 mg/mL and buffer exchanged into 50 mM HEPES (pH 8.2), 50 mM NaCl for crystallization trials. Initial crystals were grown at 12°C by mixing the protein solution with equal volume of reservoir solution (0.2 M NaBr and 20% PEG 3350). The diffraction analysis showed poor multiple diffraction spots to around 4Å. Fine tuning attempts using various additives and detergents did not improve the crystal morphology. Since crystal morphology at 12°C and 20°C were similar, further optimization attempts were performed at 20°C. A grid search using various buffers identified HAT (made by mixing equal volumes of 1M Tris (pH 8.0), 1M HEPES (pH 7.5), and 1M ADA (pH 6.5)) as the optimal buffer for crystal formation. Seeding protocols with 1:1000 diluted crystal seeds introduced to the drop after two days gave small single crystals. A grid search by varying concentration of PEG and NaBr and also varying the drop ratio generated the best crystals with a well solution containing 75 mM NaBr, 18% PEG 3350, and 50 mM HAT buffer. The drop ratio for the best crystals was 0.8 μL of protein and 0.6 μL of well solution.

The crystals were flash cooled by dipping in a well solution containing 32% PEG 3350. Diffraction datasets were collected at 100° K via Stanford Synchrotron Radiation Lightsource (SSRL) beamline 12-2 at a wavelength of 0.98 Å using PILATUS 6M detector. Data were indexed and integrated using the XDS package (Kabsch, 2010). The crystals belong to space group $P2_1$ and contain one monomer per asymmetric unit. The best crystals diffracted to around 1.7 Å and the final data (480 degrees) is processed to 1.85 Å resolution. In addition, low dose and highly redundant sulfur SAD data were collected at a wavelength of 1.55 Å by using the 5 degree inverse beam geometry (total 4670 degrees of data). The crystallographic data are summarized in Table S1.

Structure determination and refinement

The human VISTA ECD sequence was submitted to the GREMLIN server (gremlin.bakerlab.org) for co-evolution contact predictions and a list of top homology models. Ten thousand decoy structures of hVISTA were generated using Rosetta homology modeling (RosettaCM; Song et al., 2013) with the top ten VISTA homologs obtained from the GREMLIN search as templates. The initial screen running Phaser (McCoy et al., 2007) for possible molecular replacement solutions was conducted on the 10,000 structures generated from the RosettaCM run, but failed to produce definitive hits. Model convergence of the top 100 scoring RosettaCM solutions was analyzed to produce a partial consensus model (88 amino acids). An MR solution was obtained using the partial model. The model generated by MR search and Phenix (Adams et al., 2010) building resulted in a reliable structure with Rwork and Rfree of 0.48 and 0.54, respectively. Various building attempts with Phenix, Phenix-rosetta (Terwilliger et al., 2012), RosettaRemodel (Huang et al., 2011) (for generating templates for VISTA specific disulfides), and Buccaneer (Cowtan et al., 1998) programs brought the Rwork and Rfree to 0.37 and 0.41, respectively. Then, Phenix autobuilding by incorporating the sulfur SAD data, Buccaneer building, and extensive manual building resulted in Rwork and Rfree of 0.26 and 0.31, respectively. Further refinements were done by using Phenix and manual model building. The final model includes one protein monomer, two NAG molecules, and 41 water molecules in the asymmetric unit. No electron density was observed for the residues 29 – 31, and for the C-terminal residues starting from residue 152. The refinement converged to a final Rwork and Rfree of 0.18 and 0.22, respectively. There are no Ramachandran outliers and 98.6% of the residues are in the favored region. The refinement statistics are provided in Table S1. All crystal structure figures were created using PyMOL.

Structural comparisons, electrostatic surfaces, solvent accessibility, and buried surface area

Structural alignments between VISTA species were performed using both the pymol 'super' and 'align' commands. Structural comparisons between the B7 family proteins and human VISTA were performed using the TM-align online server (Zhang and Skolnick, 2005). The PDB IDs for the B7 family structures used in the comparison were PDB: 1DR9 (CD80), 5YXK (CD86), 3BP5 (PD-L2), 4Z18 (PD-L1), 4I0K (CD276).

Electrostatic surfaces were created using the 'APBS Electrostatics' plugin in PyMOL (Version 2.2.3). The program uses the pdb2pqr method (Dolinsky et al., 2007) to add hydrogens, missing atoms, and partial charges. The surface potential is then calculated by approximating the solution at each atom using the Poisson-Boltzmann equation (Jurrus et al., 2018). The charges are represented as a color spectrum where the scale is −5.00 to +5.00 k_BT/e. For solvent accessibility calculations, each residue in question was manually moved out to the solvent using Coot and then the PISA server (Krissinel and Henrick, 2007) was used to calculate the maximum accessible surface area. Then, the surface area of each residue as part of the structure was calculated and divided by the maximum to compute percent accessible.

Buried surface area of the interaction between monomer and crystal contacts was calculated using the CCP4 program Areaimol (Lee and Richards, 1971). The surface area of a single monomer by itself and the surface area of a single monomer in complex with two other symmetry molecules were calculated. The difference between the two is the buried surface area of the interaction.

Epitope mapping

Creation of a yeast-displayed human VISTA library

DNA encoding the human VISTA ECD amino acids (Phe33-Ala194, Uniprot), was cloned into the pCT yeast display plasmid (Boder and Wittrup, 1997; Chao et al., 2006) using standard Gibson cloning. An error-prone PCR library was created using WT hVISTA as a

template, and mutations were introduced across the entire gene using low-fidelity Taq polymerase (Invitrogen) and nucleotide analogs 8-oxo-dGTP and dPTP (TriLink Biotech) as described previously (Colby et al., 2004; Van Deventer and Wittrup, 2014). Three different PCR reactions of 15 cycles were performed with 1.25, 1.5, and 1.75 μM of dNTP analogs. The 1.75 μM dNTP analog library was found to have the highest percentage of single amino acid mutations. Restricting the library to single amino acid mutations allows for confident attribution of binding changes to a particular residue. This library was amplified and purified using gel electrophoresis. Empty pCT vector was cut using NheI and BamHI restriction sites. The amplified insert and cut vector were electroporated in a 5:1 DNA weight ratio into a strain of *S. cerevisiae* engineered for surface protein display (Boder and Wittrup, 2000; Van Deventer and Wittrup, 2014), where they were assembled *in vivo* through homologous recombination. Library size was determined to be $3.6x10^8$ by dilution plating.

VSTB and Ctrl antibodies

The VSTB antibody used for screening was derived from the Janssen Pharmaceuticals VSTB112 sequence (Snyder et al., 2014). We paired the VSTB112 heavy chain variable domain with the hIgG1 constant domain (Ala1-Lys330, Uniprot P01857) and paired the VSTB112 light chain variable domain with the human kappa light chain constant domain (Arg1-Cys107, Uniprot P01834). Heavy chain and light chain were individually cloned into the pAdd2 expression vector using standard Gibson cloning. VSTB was expressed in Expi293 cells with a 1:1 weight ratio of heavy chain: light chain DNA using the manufacturer's protocol. Antibody was purified from the supernatant using protein A affinity chromatography. The positive control ('Ctrl') antibody was provided by xCella Biosciences. The Ctrl antibody was tested for linear versus conformational binding to VISTA using heat denaturation on the surface of yeast. Yeast cells displaying human VISTA were incubated at room temperature or 80°C (in a thermocycler) for 30 min and then chilled on ice for 20 min. The samples were incubated with 2 nM Ctrl antibody in PBS + 0.1% BSA for 5 hr at 4 C to reach equilibrium. Yeast were washed and incubated with 1:5000 chicken anti-c-*myc* for 30 min at RT, followed by washing and staining for 20 min at 4°C with 1:250 anti-chicken 647 (abcam ab150171) for VISTA expression and 1:250 anti-mouse-488 (ThermoFisher A11059) for antibody binding. Yeast were analyzed by flow cytometry for quantitative measurements of binding and expression.

Yeast library screening

Yeast displaying hVISTA mutants that lost binding to VSTB but retained binding to Ctrl were isolated from the library using fluorescence-activated cell sorting (FACS). An alternating positive and negative sort strategy, as opposed to three-color simultaneous sorting, was used because binding of Ctrl decreased maximal binding of VSTB (Figure S3B), and therefore simultaneous incubation with both antibodies would not provide an accurate depiction of VSTB binding levels. Equilibrium sort rounds were performed in which yeast were incubated at 4°C for 12 hr in phosphate-buffered saline (PBS) containing 0.1% mg/mL BSA with the following concentrations of antibody: Sort 1, 10 nM VSTB; Sort 2, 75 nM VSTB; Sort 3, 50 nM Ctrl; Sort 4, 200 nM VSTB; Sort 5, 5 nM Ctrl. After incubation with antibody, yeast were pelleted, washed, and resuspended in PBS+BSA with a 1:5000 dilution of chicken anti-c-Myc (Invitrogen, A21281) for 30 mins at 4°C. Yeast were then washed and pelleted, and labeled on ice with 1:250 dilution of secondary antibodies for binding (anti-mouse 488, ThermoFisher A11059 or anti-human 647, ThermoFisher A21445) and expression (anti-chicken 647, abcam ab150171 or anti-chicken 488, ThermoFisher A11039). Labeled yeast were sorted by FACS using a BD Aria sorter (Stanford FACS Core Facility). Negative sort gates for sorts 1, 2, 4 and positive sort gates for sorts 3, 5 were drawn to isolate populations with desired binding characteristics. Following FACS sort 5, plasmid DNA was recovered from yeast using a Zymoprep kit (Zymo Research Corp), transformed into DH10b electrocompetent *E. coli*, and isolated using a GeneJET plasmid miniprep kit (ThermoFisher, K0503). Sequencing was performed by MCLAB (Molecular Cloning Laboratories).

Binding assays

Single alanine mutants of human VISTA (R54A, R58A, F62A, Q63A, or S124A) were generated using site-directed mutagenesis according to a standard two-stage QuikChange PCR protocol (Wang and Malcolm, 1999). PCR fragments were cloned into the pCT yeast surface display vector and individually transformed into EBY100 yeast. The genes for WT human VISTA (33-194, Uniprot) and mouse VISTA (33-191, Uniprot) were also cloned into pCT and transformed into yeast as described above. Binding assays were performed by mixing surface-displayed VISTA on yeast (~50,000 molecules/cell)(Cho et al., 1998) with a titration of target antibody concentrations (VSTB or Ctrl) in individual eppendorf tubes. Binding reactions were incubated at 4°C for 12 hr to allow interactions to reach equilibrium. Yeast were labeled with the same reagents using protocols as described for library sorts and analyzed by flow cytometry on a BD Accuri. Binding populations were gated using FlowJo software and geometric means of fluorescence were plotted against concentration and fit to a one-site specific binding curve on GraphPad Prism. Error bars represent standard deviation of the mean for duplicate measurements. Yeast-based affinity measurements are marked as 'apparent K_d' due to the limitations of the assay including the avidity effects of displaying numerous copies of the target protein and the deviation from true equilibrium due to multiple washing and labeling steps.

For enzyme-linked immunosorbent assays (ELISAs), recombinant proteins were immobilized on a 96-well flat bottom plate (Corning, CLS3595) by incubation at 4°C for 12-16 hr. VSIG3 was coated at 15 μg/mL and VSTB and Ctrl antibodies were coated at 2 μg/mL in PBS. Wells were washed with PBS + 1% Tween-20 and then blocked with PBS + 2.5% milk powder + 2.5% BSA at room temperature for 2 hr. Soluble His-tagged VISTA protein (WT or Ala triple variant) was added at varying concentrations in PBS + 0.1% BSA + 0.1% Tween-20 and the plate was incubated at room temperature for 2 hr. For VSTB pre-complexed experiments, 1 μM of VISTA was incubated with 1 nM – 5000 nM of VSTB in individual eppendorf tubes overnight and then added to VSIG3-coated ELISA plates. Binding of VISTA was detected indirectly by first adding 1:750 rabbit anti-6-HIS (Bethyl, A190-114F) and then adding 1:7500

anti-rabbit-HRP (Novus Biologicals, NB7160). Substrate solution (1-Step Ultra TMB, ThermoFisher, 34028) was added, reaction was stopped after 15 min with 2M sulfuric acid, and absorbance at 450 nM was read on a microplate reader (Synergy H4, BioTek). Absorbance values of control wells with no coated protein were subtracted from sample wells and corrected values were plotted against VISTA concentration and fit to a one-site specific binding curve on GraphPad Prism. Error bars represent standard deviation of the mean for triplicate measurements. ELISA-based affinity measurements are marked as 'apparent K_d' due to limitations of the assay including the deviation from true equilibrium due to multiple washing and detection steps.

QUANTIFICATION AND STATISTICAL ANALYSIS

All graphs and binding curve regressions were created using GraphPad Prism Version 8.0.2. The number of replicate samples in each experiment is specified in the figure legend. Error bars represent the standard deviation from the mean.

DATA AND CODE AVAILABILITY

The accession number for the coordinate and structure factor data of the human VISTA ECD structure reported in this paper is PDB: 6OIL.